

The following publication F. Yang, W. Jin, Y. Lin, C. Wang, H. Lut and Y. Tan, "Hollow-Core Microstructured Optical Fiber Gas Sensors," in Journal of Lightwave Technology, vol. 35, no. 16, pp. 3413-3424, 15 Aug.15, 2017 is available at <https://doi.org/10.1109/JLT.2016.2628092>

Hollow-core Microstructured Optical Fiber Gas Sensors

Fan Yang, Wei Jin, *Senior Member, IEEE*, Yuechuan Lin, Chao Wang, Hoi Lut Ho, and Yanzhen Tan

Abstract—Recent progress in gas detection with hollow-core microstructured optical fibers (HC-MOFs) and direct absorption/photothermal interferometry spectroscopy are reported. For direct-absorption sensors, the issue of mode interference noise is addressed and techniques to minimize such a noise are experimentally demonstrated. Large-scale drilling of hundreds of low-loss micro-channels along a single HC-MOF is demonstrated, which reduces the diffusion-limited response time from hours to ~40 seconds for sensing HC-MOFs of 2.3 meters. For photothermal interferometry sensors, novel detection configurations based on respectively a Sagnac interferometer and an in-fiber modal interferometer are proposed and experimentally demonstrated. The Sagnac configuration avoids the need for complex servo-control for interferometer stabilization while the in-fiber configuration simplifies the detection, reducing the size and cost of the sensor system. Sub-ppm gas detection can be achieved easily with photothermal interferometry spectroscopic HC-MOF sensors but is difficult to achieve for direct-absorption sensors with the current commercial HC-MOFs.

Index Terms—Optical fiber applications, optical fibers, optical spectroscopy, optical fiber measurements, gas detectors, photothermal effects.

I. INTRODUCTION

GAS detection has important applications in environmental and air-pollution monitoring, medicine, petrochemical industry and combustion processes monitoring [1-4]. There is a strong demand for trace gas detectors that can detect various molecular samples in low concentration with high accuracy. Conventional trace gas detectors include gas chromatograph [5], semiconductor [6], and electrochemical sensors [7]. Semiconductor gas sensors can achieve low ppm level sensitivity, they however suffer from drift and cross-sensitivity to other gases and changing humidity levels [8].

This paragraph of the first footnote will contain the date on which you submitted your paper for review. This work was supported in part by the National Natural Science Foundation of China (NSFC) through Grant No. 61290313, the Hong Kong SAR government through a GRF grant PolyU 152064/14E and an ITF grant ITS/348/14.

F. Yang, W. Jin, Y. Lin, H. L. Ho, and Y. Tan are with the Department of Electrical Engineering, The Hong Kong Polytechnic University, Kowloon, Hong Kong, China, and The Hong Kong Polytechnic University Shenzhen Research Institute, Shenzhen, China (e-mail: ee.yangfan@connect.polyu.hk; eejin@polyu.edu.hk; lin.yuechuan@connect.polyu.hk; echlho@polyu.edu.hk; yanzhen.tan@connect.polyu.hk).

C. Wang was with The Hong Kong Polytechnic University, Kowloon, Hong Kong, China. He is now with the School of Electrical Engineering, Wuhan University, Wuchang, Wuhan, China (e-mail: cecwang@whu.edu.cn).

Electrochemical gas sensors show relatively good selectivity, however they have limited lifetime and also have cross-responsivity to for example humidity [7]. Laser absorption spectroscopy, which relies on the “finger-print” absorption lines of molecules for identifying and detecting trace chemicals, is a powerful technique that offers high selectivity and sensitivity [9]. The employment of fiber-based technologies enables compact sensors with lower cost, immunity to electromagnetic interference, capability of operating in harsh environment and remote interrogation and multiplexed multi-point detection [10].

When a laser beam with a specific wavelength (or frequency) propagates through a gaseous medium, part of the light energy will be absorbed, as shown in Fig. 1. The transmitted optical intensity through the absorptive gas is governed by the Beer-Lambert Law.

$$I_{out}(\nu) = I_0(\nu) \exp(-\alpha(\nu)CL) \quad (1)$$

where $I_{out}(\nu)$ and $I_0(\nu)$ are the light intensities with and without absorption, ν is the frequency of the light, $\alpha(\nu)$ is the gas absorption coefficient for 100% concentration, C is the relative gas concentration, L is the length of the gas cell. The absorption spectrum and strength are unique for specific gas molecules, which can be used to identify the gas species and determine its concentration.

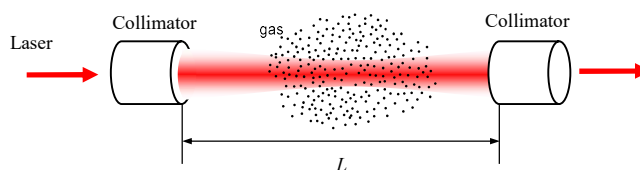


Fig. 1. Schematic of an optical absorption sensor.

A key performance indicator of gas sensors is the limit of detection (LOD), which is often expressed in terms of noise equivalent concentration (NEC) for a signal-to-noise ratio (SNR) of unity. For absorption-based sensors, the LOD is also expressed in terms of noise equivalent absorption coefficient (NEAC) [11], which is independent of absorption line-strength and reflects the capability of the optical detection system. The value of NEAC may be obtained from that of NEC by simply multiplying the peak absorption coefficient for a relative concentration of 100%.

Several review papers on the recent developments of direct-absorption optical and fiber-optic gas sensors may be

found in [8, 12-14].

Conventional direct absorption optical fiber gas sensors use open-path (bulk or micro-optic) absorption cell with optical fibers as light guides to transmit signals to/from the gas cells [15-17]. However, standard silica fibers have a transparent window from ~ 0.5 to ~ 2 μm , covering only the relatively weak absorption lines of gas molecules. These sensors have limitations in achieving higher sensitivity due to difficulty in fabricating long-path-length absorption cells with compact sizes. Very long optical path lengths may be achieved by using multi-pass optical cells such as the White cells [18], Herriott cells [19] or cavity enhanced optical cells [20]. However, these cells are bulky, expensive and need careful alignment.

Attempts were made to develop all-fiber evanescent field gas sensors with D-shaped optical fibers [21, 22]. However, the fraction of evanescent field is too small to enable any practical sensing devices with good detection sensitivity.

Small-core index-guiding photonic crystal fibers (PCFs) and suspended-core fibers have a larger fraction (e.g., 1 to 30% at 1.5 μm) of evanescent field power located in air-holes and they have been exploited for gas detection [12, 23, 24]. The first gas detection experiment was done with a 10-cm-long small-core PCF and it was predicted that ppm level gas detection could be achieved with ~ 5 m of such fiber. The response time is limited by the time for gas to diffuse into the air-holes and it was proposed to introduce multiple side-openings along the fiber to facilitate fast access to the evanescent field [23, 25].

Hollow-core microstructured optical fiber (HC-MOF) confines an optical mode within its hollow core and the optical power propagating in the central hollow core can be $>95\%$ of the total mode power [26, 27]. The state-of-the-art HC-MOFs have sufficiently low attenuation [28-31], which enables stronger light-gas interaction over a longer distance and would allow developing higher sensitivity gas sensors. There are three types of HC-MOFs that may be exploited for gas detection. The first type is a hollow-core photonic bandgap fiber (HC-PBF) (Fig. 2(a)) which has a periodic air-silica cladding structure. The air-silica cladding has a full two-dimensional photonic bandgap, within which light is prohibited to travel in the transverse direction but confined within the hollow core and propagates along the fiber with low loss [32, 33]. The other two types of HC-MOFs are Kagome fibers [34, 35] (Fig. 2(b)) and a simpler structure with a single ring of antiresonant elements [29, 36, 37] (Fig. 2(c)). Kagome cladding lattice does not have a full photonic bandgap and such a fiber guides light via inhibited coupling between the core modes and the cladding modes [34, 35]. The lowest transmission loss is reported to be 12.3 dB/km [38]. Very recently, Uebel et al. reported a broadband single-mode hollow-core fiber by resonant filtering of higher-order modes [30]. Most of the HC-MOF gas sensors reported so far used HC-PBFs, and very little work has been reported using the other two types of HC-MOFs [39]. Hence, we focus here on the HC-PBFs with a cladding structure illustrated in Fig. 2(a).

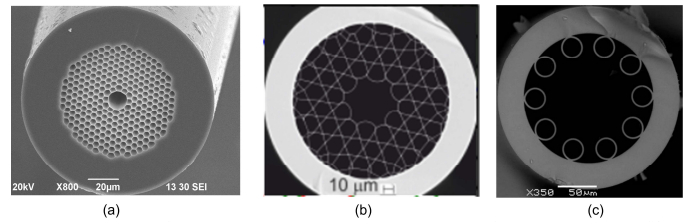


Fig. 2. Scanning electron microscope (SEM) images of (a) HC-1550-02 fiber from NKT Photonics, (b) Kagome lattice fiber [38], and (c) hollow antiresonant fiber [29].

The HC-1550-02 HC-PBF shown in Fig. 2(a) has a hollow-core diameter of ~ 11 μm and supports a few guided modes. It has a bandgap-limited transmission windows of ~ 200 nm centered around 1550 nm, and the attenuation within the window is <24 dB/km. There are other commercial HC-PBFs that have different wavelength transmission windows ranging from 440 nm to 2000 nm (HC-PBFs from NKT Photonics), covering the absorption lines of many important gases. HC-PBFs with a larger hollow-core (19-cell HC-PBF from NKT Photonics) is also commercially available and these fibers have demonstrated lower transmission loss but support a larger number of guided core modes.

The possibility of using HC-PBFs for gas detection was suggested by Cregan et al. in 1999 [26]. Hoo et al. firstly reported gas diffusion measurement with absorption spectroscopy in a HC-PBF [40]. A while later, Ritari et al. reported gas absorption measurement using HC-PBFs with transmission windows centered at 1300 and 1500 nm [41]. Since then, several research groups have used HC-PBFs for detection different gases such as C_2H_2 , C_2H_6 , CH_4 , CO_2 , NH_3 and O_2 [42-56].

Nwaboh et al. fabricated HC-PBF with transmission band in the 2 μm wavelength region. By using 5.27-m-long HC-PBF gas cell, a NEC of 311 ppm CO_2 was demonstrated, corresponding to a NEAC of 2.6×10^{-3} cm^{-1} [51]. Cubillas et al. demonstrated detection of methane gas using HC-PBFs in the 1.3 μm [53] and 1.6 μm bands [45]. For the latter case, a NEC of ~ 10 ppm methane with 5.1-m-long HC-PBF cells was achieved, corresponding to a NEAC of 1.6×10^{-6} cm^{-1} [45]. There are more works on gas detection using HC-PBFs, and they are summarized in Table II in Section IV.

The low attenuation of HC-PBFs and its capability of being coiled to small diameters (e.g., a couple of cm) with minimum additional loss [57] would in principle enable highly sensitive and compact “point” all-fiber gas sensors based on absorption spectroscopy. In combination with optical time-domain reflectometry technique, HC-PBFs would also allow distributed detection of gas concentration along a single optical fiber [12]. However, the detection limit of the HC-PBF sensors was found seriously limited by the mode interference (MI) noise [12, 55, 58]. Current commercial HC-PBFs support several groups of modes and the interference of these modes results in fluctuation of the transmitted light intensity and limits the LOD. Efforts were made to develop truly single-mode (and single polarization) HC-PBFs within which the MI could be avoided [59, 60]. However, so far there is no true single-mode HC-PBFs available on the market. The use of long (e.g., a few

meters) sensing HC-PBF also results in impractically slow response of the sensor, due to time taken for gas to get into the hollow core.

In this article, we report recent development in HC-PBF gas sensors. We start from our recent work on improving the detection sensitivity by minimizing the modal interference noise and shortening the response time by drilling large-scale micro-channels along the HC-PBFs. We then report the progress developing a novel type of HC-PBF gas sensors based on photothermal interferometry spectroscopy, compare the performances of various HC-PBF gas sensors, discuss possible future development, and conclude with a summary of the findings.

II. DIRECT ABSORPTION HC-MOF GAS SENSOR

A. Reduction of Mode Interference (MI)

1) Effect of Mode Launch, Fiber Length and Wavelength Modulation

Although the HC-PBF shown in Fig. 2(a) supports a few core modes as well as cladding modes (surface modes), the difference between the effective refractive indexes of the fundamental, higher order core modes and cladding modes are large [28]; hence coupling between these modes would usually not occur unless with extremely strong disturbances such as long period gratings are made along the fiber [61]. This means that the MI noise could be significantly reduced by avoiding the excitation of higher modes at the input end of the fiber. It has been shown that by introducing a ~ 100 μm gap between a standard single-mode fiber (SMF, SMF-28e from Corning Inc.) and a HC-PBF, it is possible to launch more favorably the fundamental mode while minimizing the higher order core modes and cladding modes and reducing the MI by a factor of 2 [62].

The losses of higher order core modes and cladding modes in a HC-PBF are larger than the fundamental mode, and hence if the HC-PBF used is sufficiently long, the higher order core modes and cladding modes could in principle be attenuated completely and no interference between different spatial modes would then be observed. However, for sensor applications which typically use a shorter length of HC-PBF, the MI would almost certainly exist. We have studied the effect of the increasing HC-PBF length on MI and found the magnitude of the MI noise is reduced by a factor 4 and 7 when the length of the HC-PBF is increased from 0.3 to 5 and 13 meters, respectively [62].

With wavelength-modulation spectroscopy (WMS), the coherent MI noise may also be reduced by selecting proper modulation parameters [63, 64], as have been done for the reducing the residual etalon effect in direct-absorption gas sensors [65]. The MI fringes have different spectral decomposition from the gas absorption signal and hence the MI noise may be further reduced by post signal processing. We have demonstrated the reduction of MI by a factor of 5 by proper wavelength modulation, and a further improvement of SNR by a factor of 3 by applying a digital low-pass filtering after lock-in detection.

With the aforementioned techniques, we have demonstrated acetylene gas detection down to ~ 1 ppm with ~ 13 -m-long sensing HC-PBF [62]. However, in many practical applications, a shorter HC-PBF is preferred for faster response and cost reduction, and it would also be better to fusion splice the sensing HC-PBF directly to single-mode transmission fibers to improve robustness. Recently we developed two novel techniques for MI reduction in shorter HC-PBF samples with SMF pigtailed. They are presented in Section II A(2) and II A(3).

2) MI Reduction with LMA-5 Fiber as Modal Filter

The LMA-5 fiber (NKT Photonics), shown in Fig. 3(a) is a true single-mode fiber. The core diameter, spacing between the cladding holes (pitch) and mode-field diameter (MFD) of the HC-1550-02 fiber and LMA-5 fiber are listed in Table I. The spatial overlap between the fundamental mode in LMA-5 and the cladding modes in HC-1550-02 is small and hence the LMA-5 fiber may be used as a modal filter to reduce the content of the cladding modes and hence the MI noise due to cladding modes.

In this paper, all the fibers are cleaved by a fiber cleaver (FC-6S, Sumitomo Electric Industries LTD.) before fusion splicing.

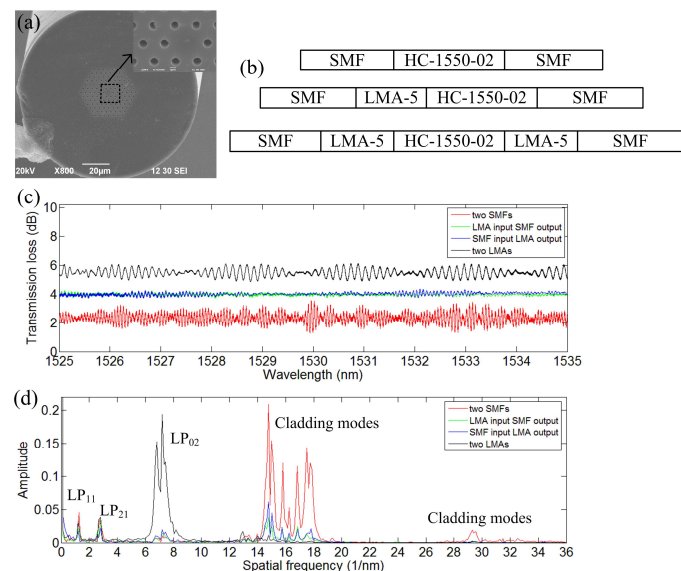


Fig. 3. (a) Cross-section of LMA-5 fiber. (b) Three HC-1550-02 samples with SMF/LMA-5 fiber pigtailed, the lengths of the HC-1550-02 fibers are ~ 30 cm. (c) Transmission spectra of the HC-1550-02 samples. (d) The Fourier transforms of the transmission spectra in (c).

TABLE I
FIBER PARAMETERS AT 1550 NM

Fiber	Core diameter (μm)	Pitch (μm)	MFD (μm)
HC-1550-02	10.9	3.8	7.5
LMA-5	4.5	2.9	4.1

We conducted experiments with three HC-1550-02 samples spliced to SMF and/or LMA-5 fibers by using an Ericsson FSU-975 fusion splicer. The sequence of the SMF, LMA-5 and

HC-1550-02 for the three fiber samples are shown in Fig. 3(b). Before fusion splicing, the end of all the fibers were cleaved by a fiber cleaver (FC-6S, Sumitomo Electric Industries). The fusion current used was low with short duration to avoid collapse of air-holes. The normalized transmission spectrums of these samples were measured by use of a wavelength-tunable external cavity diode laser (ECDL) and a photodetector. The wavelength tuning resolution was set to 1 pm. The lengths of HC-1550-02 fiber and the LMA-5 pigtailed are 30 and 10 cm, respectively.

The measured transmission spectrums of the fiber samples are shown in Fig. 3(c). The SMF/LMA-5/HC-1550-02/SMF sample was tested twice with light launched into the sample from different ends. The periodic fringes observed are due to interference between different modes and the mode contents in each of samples may be observed by the Fourier transforms of the spectrums [58, 66], as shown in Fig. 3(d).

The HC-1550-02 sample with one end spliced to a SMF and the other end to a LAM-5 demonstrated a reduction of MI by 6.7 times in decibel with additional splicing loss of 1.68 dB compared with the sample with both ends spliced to SMFs. The reduction of MI is primarily due to the reduction of cladding modes, as labeled in Fig. 3(d). The HC-1550-02 sample with both ends spliced to the LMA-5 fibers demonstrated further reduction in cladding modes, but the LP_{02} mode is excited/collected more and the peak-to-peak value of the MI increases due to interference of the fundamental core mode with the LP_{02} mode. This is because the MFD of LMA-5 fiber is smaller than the standard SMF and the mode field of LMA-5 overlaps more with the LP_{02} mode of the HC-1550-02 [62].

The splicing loss between SMF and LMA-5 fiber may be reduced to less than 1 dB by repeated arc discharges using a fusion splicer [67].

3) MI Reduction by Controlled Collapsing of Cladding Air Holes

Splicing the sensing HC-PBF to SMF transmission fibers enables robust all-fiber gas sensors. Fusion splicing could however collapse the air holes in the cladding and affect the splice loss [68]. We experimentally studied the effect of fusion splicing on MI noise and found that the MI noise could be reduced considerably without significantly increasing the splice loss.

The HC-1550-02 fiber samples were fusion spliced to SMFs at both ends by use of the Ericsson FSU-975 fusion splicer. For the splice at the output end of the HC-PBF, the fusion current used was low with short duration to prevent collapse of air-holes in the HC-PBF [67]. The input end of the HC-1550-02 fiber was however spliced to SMF with different fusion currents from 14 to 17 mA. The fusion duration was set to 0.2 s, and the offset and overlap were 45 and 10 μm , respectively.

The transmission spectrums of several samples with different splicing fusion currents applied to the input splices are shown in Fig. 4. The spectrums were measured by the same ECDL and photodetector combination as in Section II A(2)). The length of the HC-1550-02 fiber was about 57 cm and the lengths of the

SMF pigtailed were ~ 2 m. The spectrums were normalized to the source spectrum measured directly from its SMF pigtailed.

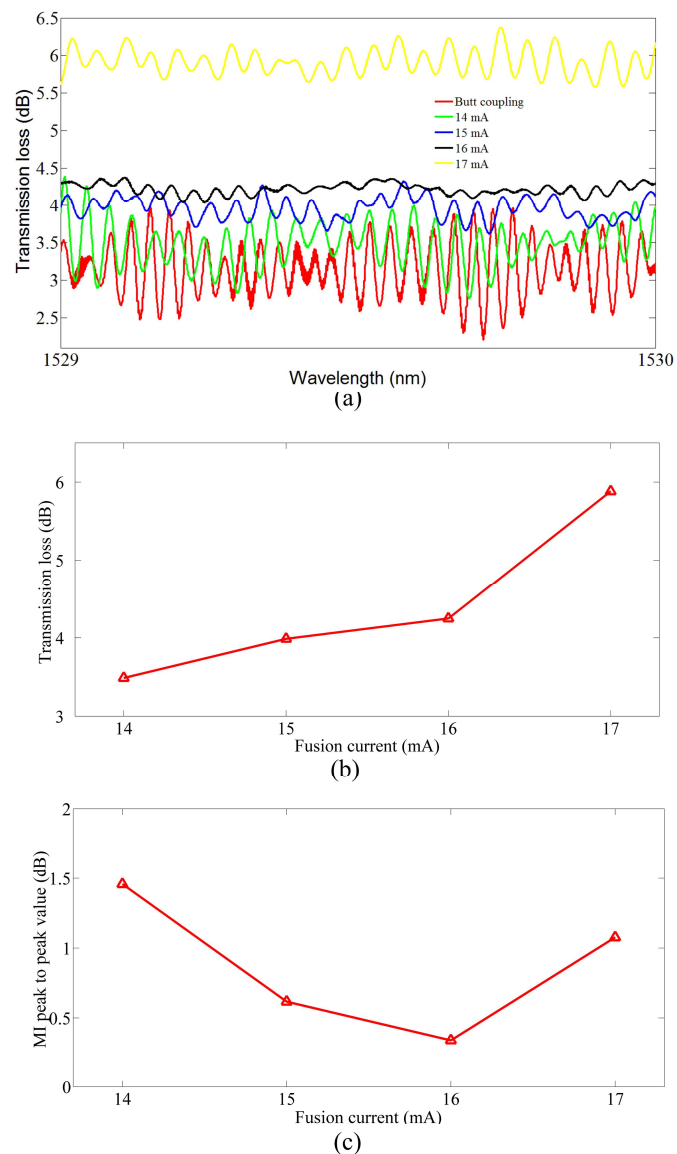


Fig. 4. (a) Measured (normalized) transmission spectrums of ~ 57 cm HC-PBF with different fusion currents from 14 to 17 mA applied to the input splice. (b) Average transmission loss in the wavelength range of 1529-1530 nm and peak-to-peak amplitude of MI as a function of fusion current.

When the sensing HC-PBF is short (< 3 m) and the ends of HC-PBF are fusion spliced with SMFs, the interference between the cladding modes and fundamental mode dominates MI [62] and results in the higher frequency oscillations shown in Fig. 4(a). However, for a fusion current of 16 mA applied to the input splice, the peak-to-peak value of the MI is reduced by 7.3 times as compared with butt-coupling and only ~ 1 dB additional loss is introduced in the wavelength range of 1529-1530 nm. The significant reduction of MI was demonstrated for several samples with lengths below 3 m, and the cladding mode power was significantly reduced by using a fusion current of 16 mA.

Figures 4(b) and 4(c) show respectively the measured average transmission loss and the peak-to-peak value of the MI

in the wavelength range of 1529-1530 nm for different fusion currents. The increase of splice loss with increasing fusion current is expected due to distortion/collapse of air-holes and the increased recess of HC-PBF at the splice joint [68].

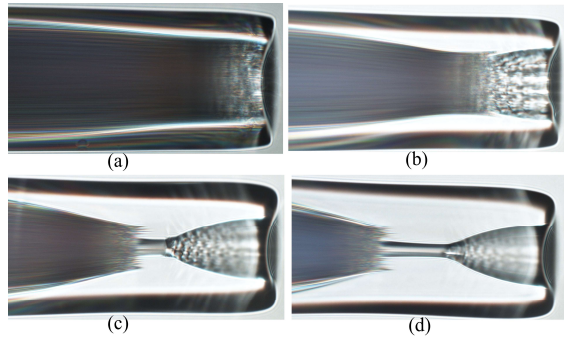


Fig. 5. Side view of HC-1550-02 samples with different fusion current applied. (a) 14 mA, (b) 15 mA, (c) 16 mA and (d) 17 mA.

To see what happened to the HC-PBF for different fusion currents, we repeated the experiments for the same fusion parameters but the SMF was withdrawn just before the start of the arc discharge. By doing so, the tip of the HC-1550-02 fiber was not spliced to the SMF but heated up by the arc discharge so that we could observe the degree of air-hole collapse for different fusion currents. Figure 5 shows the optical microscope images of the HC-1550-02 samples when after they were subjected to arc discharges with fusion currents from 14 to 17 mA. With increasing fusion currents from 14 to 16 mA, a larger degree of air-hole collapse in the cladding was observed. For 16 mA, all the cladding holes would collapse over a short section of the HC-PBF, which would induce a larger loss to the cladding modes. However, the hollow core remains relatively unaffected, and hence the core modes are relatively unaffected. The short collapse region would act as a mode filter to reduce the power of the cladding modes but not the core-modes. The side view of a typical HC-1550-02/SMF splicing joint with 16 mA fusion current is shown in Fig. 6. The extent of collapse of cladding air-holes is similar to that shown in Fig. 5(c).

When the fusion current was increased to 17 mA, the hollow core was also affected considerably, which results in a larger transmission loss to the fundamental core mode as well as increasing coupling to the higher order LP_{02} mode. Hence the MI due to interference of the fundamental and the LP_{02} mode of the HC-PBF increases, as shown in Fig. 4.

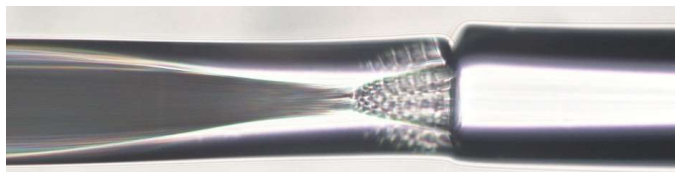
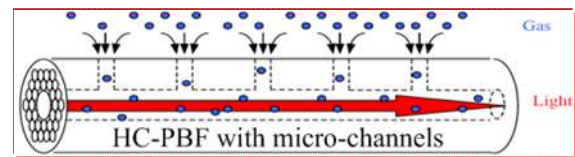
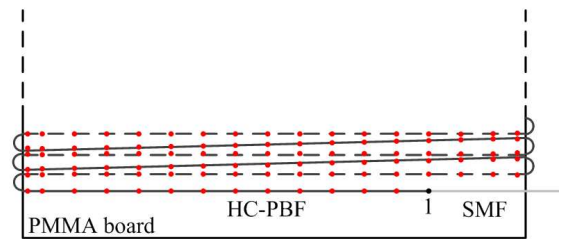


Fig. 6. Optical image of a typical HC-PBF/SMF splice.

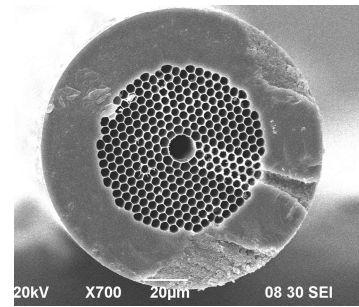
B. Improving Response Time



(a)



(b)



(c)

Fig. 7. (a) Schematic of HC-PBF with multiple micro-channels. (b) Schematic diagram of HC-PBF sensor with multiple micro-channels. Point 1 is the SMF/HC-PBF splice joint. The red dots show the drilling points of the micro-channels. Solid lines of HC-PBF are in one side of PMMA board and dotted lines of the HC-PBF are in the other side. (c) SEM image of HC-1550-02 fiber with a femtosecond-drilled micro-channel [12].

An important issue associated with the use of a long HC-PBF is the slow response limited by the time taken for gas to get into the hollow core. The fabrication of side-holes or micro-channels along the sensing HC-PBF would enable faster gas diffusion into the hollow core and hence improve the sensor response time. Figure 7(a) shows the schematic of HC-PBF with multiple micro-channels.

Different techniques have been used to fabricate micro-channels such as using a 193 nm ArF laser [69], a heating and pressure assisted method [70], a focused ion beam milling technique [71, 72] and a femtosecond laser [56, 73, 74]. Among the various approaches studied, the drilling of low-loss micro-channels directly on HC-PBFs with a femtosecond infrared laser seems an attractive approach with potential for fast and large-scale manufacturing capability [12]. Hensley et al. [73] fabricated six micro-channels in a 33-cm-long HC-PBF by a femtosecond laser. Index-matching fluid was used to circumvent the fiber and to keep the tight focus of femtosecond laser pulses into the fiber. The loss induced by each channel was estimated to be 0.35 dB. van Brakel et al. [74] drilled micro-channels in both acrylate-coated and uncoated HC-PBFs. The success in fabrication of micro-channels in the coated HC-PBF is beneficial for improving the mechanical strength of the sensor.

We studied the use of femtosecond infrared laser to drill micro-channels in HC-1550-02 fiber and investigated the

impact of drilling micro-channels on the loss and MI. Before drilling, HC-1550-02 fibers were firstly fusion spliced to SMF pigtailed at both ends, then fixed onto a PMMA board (20cm×10cm×1cm) as illustrated in Fig. 7(b). The black dot marked in Fig. 6(b) represents a SMF/HC-1550-02 fiber splice joint, while the red dots indicate the positions where micro-channels were to be fabricated. Near the edge of the PMMA board, a short length (~2.5 cm) of HC-PBF was bent and the bending loss was found negligible. The micro-channels were fabricated in the straight portion of the HC-PBF. The SMF pigtailed were connected to a broadband light source and an optical spectrum analyzer respectively and used monitor in-situ the transmission spectrum during the fabrication of micro-channels. The experimental setup used for drilling the micro-channels into the HC-PBF was similar to that reported in [12]. Femtosecond laser pulses with 120 fs duration and a repetition rate of 1 kHz were produced at central wavelength of 800 nm by a Ti: sapphire laser system. The laser beam was focused on the HC-PBF with a spot size of ~2 μm by a microscope objective (×20, NA=0.5, working distance=2.1 mm). The intensity of the laser beam was controlled using a half-wave plate and a linearly polarizer. The fiber sample was mounted on a computer-controlled, three-axis translation stage with 100 nm resolution. With the assistant of a Nikon 80i optical microscope and a CCD camera, we could accurately determine and clearly observe the focus position. To fabricate a micro-channels, femtosecond laser pulses with pulse energy of ~5 μJ were focused on the fiber surface for ~30 s. A typical micro-channel from fiber surface to fiber core is shown in Fig. 7(c).

Figures 8(a) and 8(b) show the normalized transmission spectra for different numbers of drilled micro-channels for a 2.3-m-long and a 3.2-m-long HC-PBF, respectively. For the 2.3-m-long HC-PBF sample, the average loss from 1525.5 to 1535 nm for 80 side-holes was measured to be ~0.78 dB, giving an average loss of less than 0.01 dB per channel. For the 3.2-m-long HC-PBF sample, the mean loss of the micro-channels or holes is less than 0.027 dB per hole for 144 holes. These low-loss holes would enable fast gas sensor based on direct absorption spectroscopy as described in this section, as well as photothermal interferometry sensors as will be described in Section III.

We conducted gas detection experiment with a 2.3-m-long HC-1550-02 fiber sample with 242 micro-channels made along the HC-PBF. The micro-channels were made in pairs with the two holes of a pair separated by ~100 μm, while the interval between the pairs of ~2 cm.

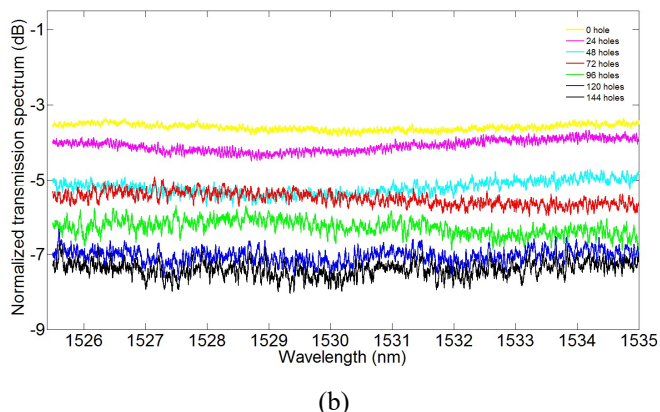
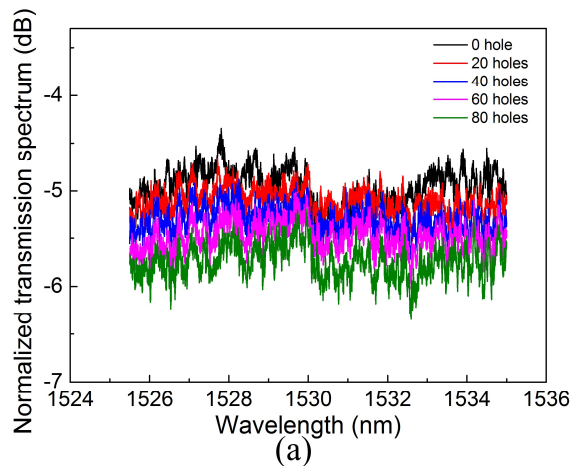


Fig. 8. Normalized transmission spectra of (a) a 2.3-m-long HC-PBF and (b) a 3.2-m-long HC-PBF with multiple micro-channels. The spectra were recorded with an OSA with 0.01 nm wavelength resolution.

To test the response time, we put the HC-PBF gas cell into a 20cm×20cm×10cm gas chamber operating at atmospheric condition. The target gas was 0.5% acetylene balanced by high purity nitrogen. The HC-PBF sample was connected to a DFB laser and a photodetector. The output signal from the photodetector during the gas loading process is shown in Fig. 9, where the wavelength of the DFB laser was tuned to the P(9) absorption line center of acetylene at 1530.37 nm. The response time t_{90} , which is defined as the time taken to reach 90% of the applied concentration [75], is measured to be ~40 s. It would take much longer (several hours) if no micro-channels were drilled on the fiber [23].

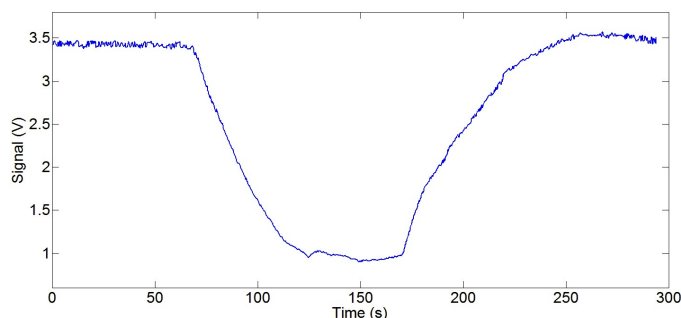


Fig. 9. Output signal with gas loading when the laser wavelength was tuned to the absorption peak at 1530.37 nm. At ~75 s, the gas was loaded into the gas chamber. At ~170 s, we stop the gas loading and open the cover of the gas chamber to allow gas to diffuse out from the chamber.

III. PHOTOTHERMAL SPECTROSCOPY WITH HOLLOW-CORE FIBERS

Direct absorption HC-PBF gas sensors are intensity-based sensors and relative simple in configuration. However, with the current commercial HC-MOFs, the LOD is primarily limited by the MI noise [55, 62] and has a value of ~ 1 ppm acetylene in terms of NEC or $1.2 \times 10^{-6} \text{ cm}^{-1}$ in terms of NEAC. We recently studied photothermal (PT) effect in a gas-filled HC-PBF and found the absorption-induced phase change due to PT effect could be exploited to develop interferometric optical fiber gas sensors with ultra-sensitivity and dynamic range [10]. In this section, we summarize the basics of the method and report the results of recent developments in alternative and more practical phase detection techniques for such PT gas sensors.

A. Basics of Photothermal Interferometry

The basis of PT spectroscopy is the photo-induced change in the thermal state of the sample. When the input light is absorbed by the gas molecules, the molecules are excited to higher energy states and then return to their initial state via molecular collision. This process results in heating [76] and changes the refractive index of the gas sample.

PT interferometry (PTI) measures the change of the sample's refractive index (RI) through the optical phase modulation. PTI typically uses a pump-probe configuration. When a modulated pump (either in wavelength or in intensity) and a probe beam propagate along the same path, the induced phase modulation in the probe beam may be expressed as [76]:

$$\Delta\phi \propto \frac{P_{pump}}{\pi\omega^2} l\alpha(\lambda), \quad (2)$$

where P_{pump} is the power and ω the mode field radius of modulated pump beam, l the interaction length, $\alpha(\lambda)$ absorption coefficient of the gas.

PTI has been studied for the detection of gases or chemical vapors such as methanol [77], ammonia [78], sulfur hexafluoride [79], hydrazines [80], as well as aerosols [81] and nitrogen dioxide [82] with very high sensitivity. Previous works however used bulk optical gas cells and mid-infrared pump laser sources. These free-space systems are complex, bulky, expensive and incompatible with fiber-optic systems. Until very recently, no sensitive PTI-based gas sensors operating in the near-infrared telecom wavelength range were reported, probably due to the very small phase modulation resulted from the weak absorption of gases within this wavelength region.

B. PT Phase Modulation in HC-PBF

HC-PBF provides an efficient platform for non-linear light-gas interaction and enables significant enhancement of PT phase modulation. As shown in Fig. 10, when a periodically modulated pump beam is co-propagating with a probe beam in a gas-filled HC-PBF, the phase of the probe is modulated due to periodic pump absorption within the HC-PBF.

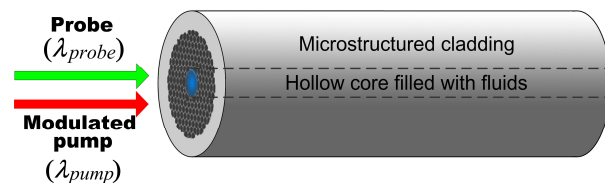


Fig. 10. PT phase modulation in HC-PBF [83]. Pump and probe light beams propagate through the same gas-filled HC-PBF.

The radius of the fundamental mode in a HC-PBF is much smaller than a typical free-space beam, this means that the phase modulation, according to Eq. (2), can be made significantly higher than a free-space case for the same pump power level and the same interaction length. The transmission loss of the fundamental mode in a HC-PBF is very low [32], meaning that a long HC-PBF may be used as the gas cell that further enhances the phase modulation. Hence the use of HC-PBF would enable sufficient phase modulation with a relatively low-power pump operating at a wavelength with relatively weak gas absorption. This would allow the use of laser sources and photonic components operating at the near-infrared wavelength range that are typically more cost-effective, compact and compatible with the standard telecommunication optical fiber systems.

However, the phase modulation process in a HC-PBF could be more complex than in a free-space beam. The absorption-induced periodic heating in the hollow core modulates the temperature, density and pressure distribution in the hollow core, which would not only modulate the RI of the gas within the hollow core, but also perturb the transverse and longitudinal dimensions of the HC-PBF. We studied experimentally and numerically the phase sensitivity of the fundamental mode of a HC-PBF to internal gas pressure [84] and found that the phase changes due to the pressure-induced transverse dimension and fiber length (longitudinal) changes are at least two orders of magnitude smaller compared with that due to the gas RI change. More work is currently directed to understand gas thermal dynamics in the hollow core and its effect on the PT phase modulation.

C. Phase Detection Techniques

In our first demonstration of PT HC-PBF gas sensors, an optical fiber Mach-Zehnder interferometer (MZI) was used to detect the PT phase modulation. The sensing HC-PBF forms one arm of the fiber-optic MZI while the reference arm is made of a standard SMF. To perform sensitive phase demodulation, the MZI needs to operate around a quadrature point where the phase to intensity conversion is linear and most efficient (Fig. 11). Operating at other point (e.g., point B in Fig. 11) would cause signal fading or distortion. However, it is well known that operating point of a fiber MZI is unstable and sensitive to environmental disturbance. Hence active feedback control is needed to maintain the operation around the quadrature point [85]. With a stabilized MZI, we have demonstrated ppb level detection of acetylene and a dynamic range of ~ 6 orders of magnitude, ~ 3 orders better than the previous direct

absorption-based HC-PBF sensors [10].

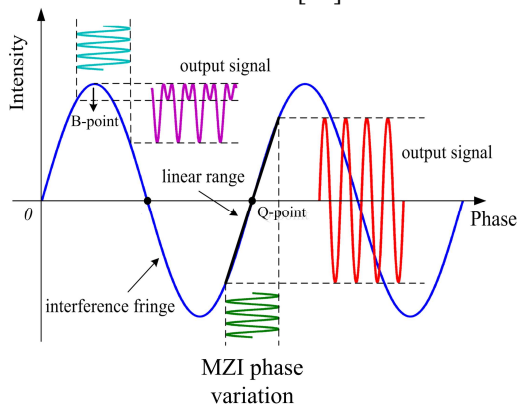


Fig. 11. Illustration of the phase versus intensity of a MZI at different operating points.

However, the fiber MZI configuration is not ideal since electronic feedback needed to maintain quadrature operation. Furthermore, it is not a universal demodulation system since the use of sensing HC-PBF with different length would change the optical path difference (OPD) between the two arms, which results in changes in the operating point as well as the noise performance. The system needs to be re-set or re-calibrated for different lengths of HC-PBFs and each time when the system is switched off. The use of phase generated carrier (PGC) demodulation could overcome the problem of electronic feedback but the OPD related issue remains. We recently worked on developing alternative detection techniques to enable simpler/more practical gas sensors. One technique uses a fiber Sagnac interferometer to passively achieve quadrature operation, and the operating point is stable and remains unchanged regardless the length change of the sensing HC-PBF. The other is a simpler scheme that uses an in-fiber modal interferometer for phase demodulation. These techniques are described in Section III C(1) and III C(2), respectively.

1) Demodulation with a Sagnac Interferometer

A fiber Sagnac interferometer is a single fiber interferometer in which counter-propagating beams travel through the same fiber loop. It has the advantage of zero OPD regardless of the fiber loop length and is much more stable than a fiber MZI when subjected to environmental disturbance [86, 87].

Figure 12 shows the Sagnac interferometer for PT phase detection using a 3×3 coupler. A 0.62-m-long HC-1550-02 fiber was fusion spliced to SMF at both ends with one end using controlled collapsing of air holes to reduce MI between cladding modes and fundamental core modes.

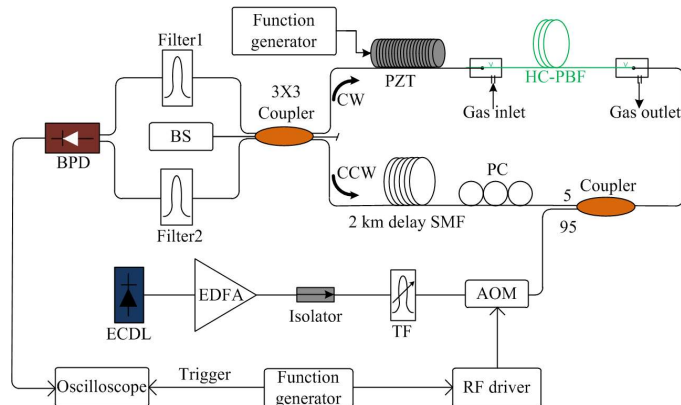


Fig. 12. Phase detection experimental setup with Sagnac interferometer combined with a 3×3 coupler. BS, broadband source; PZT, piezoelectrical transducer; PC, polarization controller; ECDL, external cavity diode laser; EDFA, erbium doped fiber amplifier; TF, tunable filter; AOM, acousto-optic modulator; BPD, balanced photodetector; CW, clockwise wave; CCW, counter clockwise wave; RF, radio frequency. The tunable filter is used to remove the amplified spontaneous emission noise. Filter1 and filter2 are used to remove the pump light.

15 micro-channels were drilled along this HC-PBF sample to improve the response time. A broadband source (HY-SLED, HOYATEK LTD.) with 65 nm bandwidth centered at 1550 nm was used as the probe source to reduce the effect of coherent backscattering noise in Sagnac interferometer. The output of the 3×3 coupler have 120 degree phase difference with each other [87]. And the use of a balanced photodetector as showing in Fig. 12 gives us a stable output which is proportional to the sine of the phase difference between the counter-propagating beams in the Sagnac loop. The balanced photodetector can also significantly reduce the laser intensity noise [88, 89]. The phase difference between the counter-propagating beams is maximum at proper frequency when $\sin(\pi f_m \Delta \tau_g) = 1$ [87], where f_m is the proper frequency and $\Delta \tau_g$ the time delay between the counter-propagating beams. Then the proper frequency can be calculated to be 50 kHz with ~2 km total fiber length (only considering the 2 km SMF shown in Fig. 12 and neglecting the SMF pigtail and HC-PBF sample).

Before the gas detection experiment, we calibrated the Sagnac interferometer with a piezoelectrical transducer (PZT) which was driven by a sinusoidal wave. We increased the PZT drive voltage from zero until the output of the oscilloscope waveform looked like the one shown in Fig. 13(a). The voltage is 5.95 V and the induced peak phase modulation is π rad (i.e., the peak-to-peak phase modulation is 2π rad). The voltage applied to the PZT can then be reduced by a factor of 100π such that the peak phase modulation is 0.01 rad and in the small signal regime where $\sin(\Delta\phi) \approx \Delta\phi$.

The output of the balanced photodetector was then measured by an electrical spectrum analyzer with resolution bandwidth of 10 Hz. The black line in Fig. 13(b) is the power spectrum when the pump is off and the peak value of the PZT induced phase modulation is 0.01 rad. The peak value at 50 kHz is -55.93 dBm. When the PZT is off and the pump light is on (modulated by an acousto-optic modulator), the peak value is -74.46 dBm. The corresponding phase change is 0.012 rad. This phase change is

believed to be the Kerr induced phase change. By calculating the power of pump light and the pump-probe interaction length in the Sagnac interferometer, the cross-phase modulation amplitude can be estimated by [90] (suppose the polarization states of both the pump and probe light are parallel)

$$\Delta\phi_{XPM} = \frac{2\pi}{\lambda_{probe}} 2n_2 \frac{P_{pump}}{A_{eff}} L^* \quad (3)$$

where $\Delta\phi_{XPM}$ is the phase change due to cross-phase modulation, λ_{probe} is the wavelength of the probe light, n_2 is the nonlinear coefficient of silica, P_{pump} is the pump power and A_{eff} is the effective area of the pump beam, L^* is the interaction length of the pump beam and probe beam.

The calculated phase change due to cross-phase modulation is ~ 0.001 rad which is accordance with the experimentally measured value. We neglected the self-phase modulation because the power of the probe light is much smaller than the pump light. We also neglect the Kerr effect induced phase change due to hollow-core fiber since nonlinear coefficient of air is ~ 3 orders of magnitude smaller than silica [91].

When the PZT drive voltage is zero, the intensity of pump light is modulated by an acousto-optic modulator, and the 0.62-m-long HC-PBF is filled with 100 ppm acetylene balanced by nitrogen. The peak value is -82.19 dBm (blue line in Fig. 13(b)). The peak intensity of the pump light input to HC-PBF is estimated to be 28.5 mW. This phase change is due to two reasons, one is the cross-phase modulation and the other is the PT induced phase change (Eq. (4)). The PT induced phase change has negative sign because absorption of pump light in the hollow core would reduce the RI of the probe light and hence the PT phase shift is opposite with pump intensity.

$$\Delta\phi = \Delta\phi_{XPM} - \Delta\phi_{Photothermal} \quad (4)$$

where $\Delta\phi$ is the total phase change and $\Delta\phi_{Photothermal}$ is the PT induced phase change. The intensity of signal shown in electrical spectrum analyzer is proportional to the absolute value of the total phase change. In this situation, the PT induced phase change is calculated to be 7.1×10^{-4} rad. The normalized PT induced phase shift is then estimated to be 4×10^{-7} rad/(ppm \cdot mW \cdot m) for 50 kHz pump intensity modulation.

The phase detection performance of the Sagnac interferometer can be estimated to be 5.5×10^{-6} rad/Hz $^{1/2}$ from the 0.01 rad signal and detection bandwidth. So the NEC is estimated to be 775 ppb (the corresponding NEAC is 1×10^{-6} cm $^{-1}$) for 1 Hz detection bandwidth.

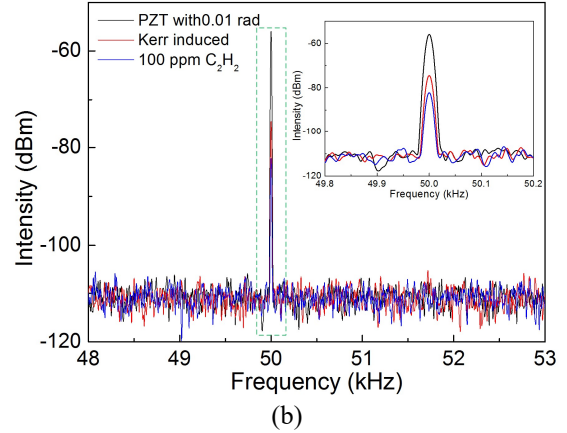
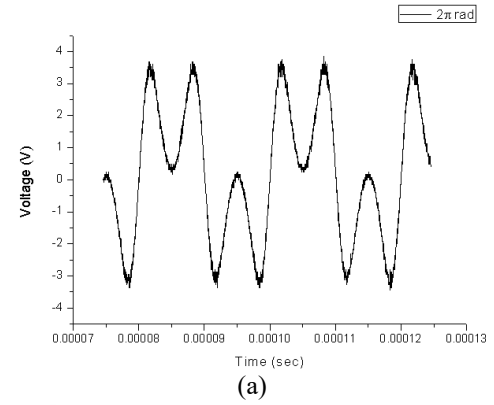


Fig. 13. (a) Output waveform observed from an oscilloscope when the peak value of the PZT induced phase modulation is π rad (peak-to-peak phase modulation is 2π rad). (b) Power spectrum of the Sagnac interferometer output measured with an electrical spectrum analyzer. Black line, when the peak value of PZT induced phase modulation is 0.01 rad; red line, when the PZT is off and the pump light is on; blue line, when the PZT is off, the pump light is on and the HC-PBF is filled with 100 ppm acetylene gas. The peak pump power delivered to HC-PBF is estimated to be 28.5 mW. The intensity of pump light is modulated by square wave with a repetition rate of 50 kHz.

2) Demodulation with In-Fiber Modal Interferometer

The PT gas detection can also be implemented with an in-fiber MZI. The in-fiber MZI use the fundamental core mode as the sensing arm and the cladding modes as the reference arm.

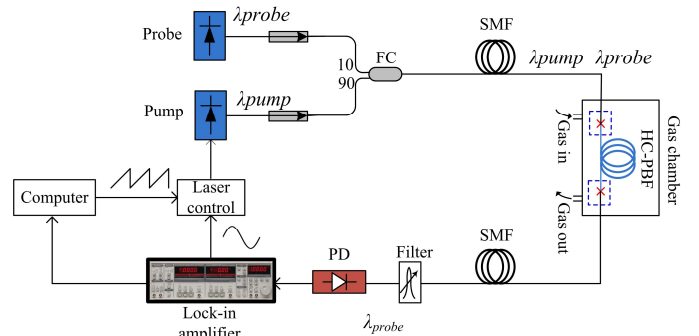


Fig. 14. Experimental setup for in-fiber MZI [92]. The fundamental mode of HC-PBF is used as sensing arm while the cladding modes of HC-PBF as reference arm. FC, fiber coupler; PD, photodetector.

Figure 14 shows experimental setup for in-fiber MZI. A 0.3-m-long HC-1550-02 fiber was butt-coupled to two FC/APCs at both ends. The gaps between HC-PBF and the two

FC/APCs are ~ 10 μm . These two FC/APCs are used at the launching and receiving ends to reduce Fabry-Perot interference due to reflections at the connecting joints and increase the excitation of cladding modes [92]. A DFB laser with wavelength at ~ 1530.37 nm was used as a pump laser and an ECDL with wavelength at 1556.58 nm was used as a probe laser. Output from PD contains the PT-induced phase modulation signal. The driving current of the DFB is modulated at 51 kHz by use of the internal signal generator of the lock-in amplifier.

Before the gas detection experiment, the transmission spectrum of our sample was measured and shown in Fig. 15 with wavelength resolution of 0.001 nm. The average spacing between adjacent fringe peaks is calculated to be ~ 70 pm, which is in accordance with the beating between fundamental core mode and cladding modes for a 0.3 -m-long HC-PBF [62]. Heat which is generated when the gas molecules absorb the pump light would induce the phase modulation of the propagating modes. Because of the perfect overlap of the propagating core modes and gas in the hollow core, the phase change of the fundamental core mode is larger than that of the cladding modes which results in a phase difference. The in-fiber modal interferometer was probed by an ECDL with its wavelength tuned to the steepest point in the transmission spectrum, i.e., 1556.58 nm, as shown in Fig. 15.

Figure 16(a) shows the second-harmonic lock-in outputs (lock-in amplifier R value) for different pump power levels delivered to the HC-PBF when the pump wavelength was tuned across the P(9) line of acetylene and the HC-PBF was filled with 7500 ppm acetylene balanced by high purity nitrogen. For the pump power of 14.9 mW, the SNR is calculated to be ~ 7517 according to Fig. 16(b). The NEC is estimated to be ~ 1 ppm ($\sim 1.2 \times 10^{-6}$ cm^{-1} in terms of NEAC) for a detection bandwidth of ~ 0.1 Hz. This simple sensor configuration would allow compact novel gas sensors to be built along a single optical fiber cable and remote detection capability.

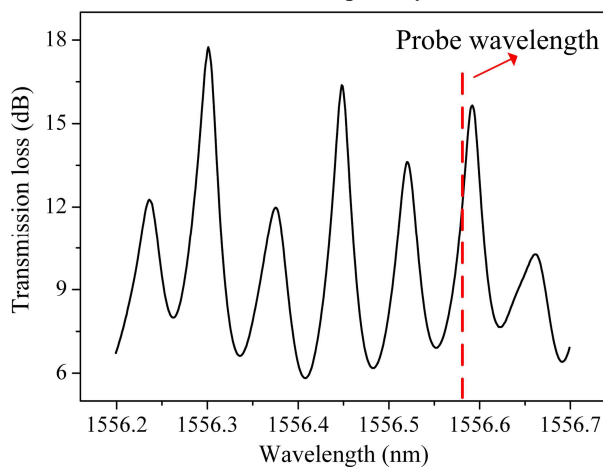


Fig. 15. Transmission spectrum of the SMF/HC-PBF/SMF sample.

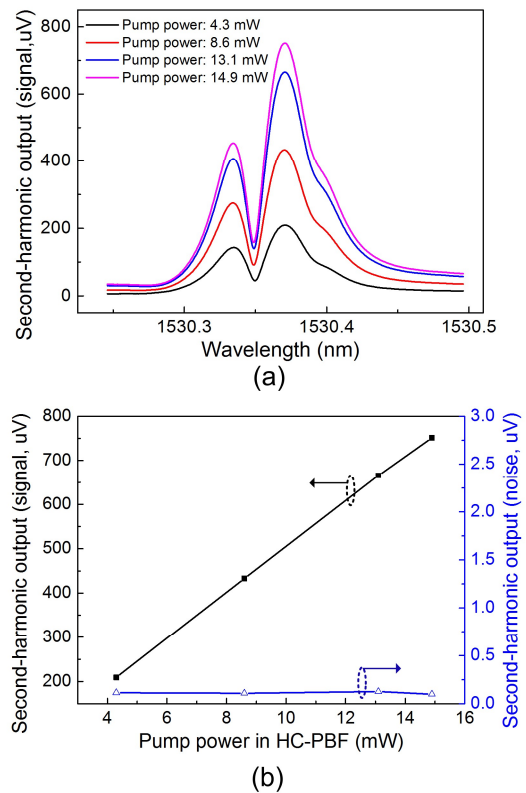


Fig. 16. Experimental results for 30 -cm-long HC-PBF filled with 7500 ppm acetylene gas balanced by nitrogen. (a) $2f$ lock-in signal output (R value) with different pump power delivered into HC-PBF. (b) $2f$ signal and the standard deviation of the noise as functions of pump power level.

IV. COMPARISON OF DIFFERENT HC-PBF SENSORS

The recent published results of gas sensors based on HC-PBFs are summarized in Table II. With WMS and optimized system parameters, the best result achieved for direct-absorption gas sensors is ~ 1 ppm acetylene in terms of NEC or 1.2×10^{-6} cm^{-1} in terms of NEAC [62]. It is relatively easy to achieve the same level of NEAC even with the simplest all-fiber PT gas sensor as shown in Fig. 14. Recently an in-fiber Fabry-Perot interferometer (FPI) based PTI gas sensor has demonstrated a NEAC of 1.4×10^{-7} cm^{-1} [93], about ten times better than previous direct absorption sensors. The direct-absorption and PT gas sensors discussed here are only suitable for absorptive molecules. Raman spectroscopy is a more versatile tool for analyzing molecules and materials and may be used to detect gas molecules with no or weak absorption as long as they have Raman-active transitions [94]. However, the sensitivity of HC-PBF Raman gas sensors is limited to ~ 100 - 1000 ppm, probably due to the small Raman scattering coefficient.

TABLE II
DETECTION LIMITS OF HC-PBF GAS SENSORS

Gas type	Wavelength (μm)	Gas cell	Technique	Integration time (s)	NEC (ppm)	NEAC (cm ⁻¹)
Methane [95]	1.666	13.7 cm HC-PBF	WMS	Not stated	158	1.8×10 ⁻⁵ *
Methane [45]	1.645	5.1 m HC-PBF	DAS	Not stated	10	1.6×10 ⁻⁶
Carbon dioxide [51]	2.005	5.27 m HC-PBF	DAS	0.018	311	2.6×10 ⁻³ *
Methane [56]	1.665	7 cm HC-PBF	DAS	Not stated	647	7.4×10 ⁻⁵ *
Acetylene [46]	1.53037	27 m HC-PBF	DAS	Not stated	50	5.8×10 ⁻⁵ *
Ethane [96]	3.35	5.69 m HC-PBF	DAS	Not stated	0.9	4.6×10 ⁻⁵ *
Acetylene [62]	1.53037	13 m HC-PBF	WMS	1	1	1.2×10 ⁻⁶ *
Acetylene [10]	1.53037	10 m HC-PBF	PTI (MZI)	1	0.002	2.3×10 ⁻⁹
Acetylene (this paper)	1.53037	0.3 m HC-PBF	PTI (in-fiber MZI)	1	1	1.2×10 ⁻⁶
Acetylene (this paper)	1.53037	0.62 m HC-PBF	PTI (Sagnac)	1	0.775	9.3×10 ⁻⁷
Acetylene [93]	1.53037	0.02 m HC-PBF	PTI (FPI)	77	0.117	1.4×10 ⁻⁷
Methane [97]	0.5145	1 m HC-PBF	RS	20	164	N. A.
Carbon dioxide [98]	0.5145	1 m HC-PBF	RS	0.03	93	N. A.
Hydrogen [99]	1.064	4.5 m HC-PBF	RS	0.03	535	N. A.

*NEA data were calculated from NEC data and the absorption line strength from HITRAN database [100]. WMS – wavelength modulation spectroscopy, DAS – direct absorption spectroscopy, PTI – photothermal interferometry, MZI – Mach Zehnder interferometer, FPI – Fabry-Perot interferometer, RS – Raman spectroscopy.

improvement in performance is possible by for example using a higher power pump laser.

V. CONCLUSIONS

In conclusion, we have reported recent developments in HC-MOFs gas sensors based on direct absorption and PTI. For direct-absorption sensors, the issues of MI noise in HC-PBF are addressed and techniques to minimize such a noise are experimentally demonstrated. Large-scale drilling of hundreds of low-loss micro-channels along single HC-MOFs is demonstrated. With such fibers, diffusion-limited response time of ~40 seconds was demonstrated. For PTI sensors, novel detection configurations based on a Sagnac interferometer and an in-fiber modal interferometer are experimentally demonstrated. The Sagnac configuration avoids the need for complex servo-control to stabilize the interferometer and could be used as a universal instrumentation to demodulate PTI sensors made with different lengths of HC-MOFs. The in-fiber configuration simplifies the detection system considerably, reducing the size and cost of the sensor system. With PTI, HC-MOF gas sensors could easily achieve sub-ppm detection limit, which is difficult to achieve with direct absorption sensors with the current commercial HC-MOFs. The research of HC-MOF PTI sensors is continuing and further

REFERENCES

- [1] P. A. Martin, "Near-infrared diode laser spectroscopy in chemical process and environmental air monitoring," *Chem. Soc. Rev.*, vol. 31, pp. 201-210, 2002.
- [2] T. H. Risby and S. F. Solga, "Current status of clinical breath analysis," *Appl. Phys. B-Lasers Opt.*, vol. 85, pp. 421-426, 2006.
- [3] D. E. Vogler and M. W. Sigrist, "Near-infrared laser based cavity ringdown spectroscopy for applications in petrochemical industry," *Appl. Phys. B-Lasers Opt.*, vol. 85, pp. 349-354, 2006.
- [4] U. Willer, M. Saraji, A. Khorsandi, P. Geiser, and W. Schade, "Near- and mid-infrared laser monitoring of industrial processes, environment and security applications," *Opt. Lasers Eng.*, vol. 44, pp. 699-710, 2006.
- [5] D. E. Matthews and J. M. Hayes, "Isotope-ratio-monitoring gas chromatography-mass spectrometry," *Anal. Chem.*, vol. 50, pp. 1465-1473, 1978.
- [6] D. E. Williams, "Conduction and gas response of semiconductor gas sensors," in *Solid State Gas Sensors*, P. T. Moseley and B. C. Tofield, Eds., Bristol: Adam Hilger, 1987.
- [7] E. Bakker, "Electrochemical sensors," *Anal. Chem.*, vol. 76, pp. 3285-3298, 2004.
- [8] J. Hodgkinson and R. P. Tatam, "Optical gas sensing: a review," *Meas. Sci. Technol.*, vol. 24, p. 012004, 2013.
- [9] W. Demtroder, *Laser Spectroscopy: Basic Concepts and Instrumentation*, 5th ed. Berlin: Springer-Verlag, 2015.

- [10] W. Jin, Y. Cao, F. Yang, and H. L. Ho, "Ultra-sensitive all-fibre photothermal spectroscopy with large dynamic range," *Nat. Commun.*, vol. 6:6767, 2015.
- [11] A. C. Boccara, W. Jackson, N. M. Amer, and D. Fournier, "Sensitive photothermal deflection technique for measuring absorption in optically thin media," *Opt. Lett.*, vol. 5, pp. 377-379, 1980.
- [12] W. Jin, H. L. Ho, Y. C. Cao, J. Ju, and L. F. Qi, "Gas detection with micro- and nano-engineered optical fibers," *Opt. Fiber Technol.*, vol. 19, pp. 741-759, 2013.
- [13] Y. Zhao, L. Bai, Y.-N. Zhang, W. Hou, and Q. Wang, "Review on structures and principles of gas cells in the absorption spectrum-based optical fiber gas sensor systems," *Instrum. Sci. Technol.*, vol. 40, pp. 385-401, 2012.
- [14] A. M. R. Pinto and M. Lopez-Amo, "Photonic crystal fibers for sensing applications," *J. Sens.*, vol. 2012, pp. 1-21, 2012.
- [15] K. Chan, H. Ito, H. Inaba, and T. Furuya, "10 km-long fibre-optic remote sensing of CH₄ gas by near infrared absorption," *Appl. Phys. B-Lasers Opt.*, vol. 38, pp. 11-15, 1985.
- [16] J. P. Dakin, C. A. Wade, D. Pinchbeck, and J. S. Wykes, "A novel optical fibre methane sensor," in *Proc. SPIE 0734*, 1987, pp. 254-260.
- [17] B. Culshaw, G. Stewart, F. Dong, C. Tandy, and D. Moodie, "Fibre optic techniques for remote spectroscopic methane detection—from concept to system realisation," *Sens. Actuators B-Chem.*, vol. 51, pp. 25-37, 1998.
- [18] J. U. White, "Very long optical paths in air," *J. Opt. Soc. Am.*, vol. 66, pp. 411-416, 1976.
- [19] D. R. Herriott and H. J. Schulte, "Folded optical delay lines," *Appl. Opt.*, vol. 4, pp. 883-889, 1965.
- [20] D. Romanini and K. K. Lehmann, "Ring - down cavity absorption spectroscopy of the very weak HCN overtone bands with six, seven, and eight stretching quanta," *J. Chem. Phys.*, vol. 99, pp. 6287-6301, 1993.
- [21] B. Culshaw, F. Muhammad, G. Stewart, S. Murray, D. Pinchbeck, J. Norris, et al., "Evanescent wave methane detection using optical fibres," *Electron. Lett.*, vol. 28, pp. 2232-2234, 1992.
- [22] G. Stewart, F. A. Muhammad, and B. Culshaw, "Sensitivity improvement for evanescent-wave gas sensors," *Sens. Actuators B-Chem.*, vol. 11, pp. 521-524, 1993.
- [23] Y. L. Hoo, W. Jin, C. Shi, H. L. Ho, D. N. Wang, and S. C. Ruan, "Design and modeling of a photonic crystal fiber gas sensor," *Appl. Opt.*, vol. 42, pp. 3509-3515, 2003.
- [24] T. M. Monro, S. Warren-Smith, E. P. Schartner, A. François, S. Heng, H. Ebendorff-Heidepriem, et al., "Sensing with suspended-core optical fibers," *Opt. Fiber Technol.*, vol. 16, pp. 343-356, 2010.
- [25] H. L. Ho, Y. L. Hoo, W. Jin, J. Ju, D. N. Wang, R. S. Windeler, et al., "Optimizing microstructured optical fibers for evanescent wave gas sensing," *Sens. Actuators B-Chem.*, vol. 122, pp. 289-294, 2007.
- [26] R. F. Cregan, B. J. Mangan, J. C. Knight, T. A. Birks, P. S. J. Russell, P. J. Roberts, et al., "Single-mode photonic band gap guidance of light in air," *Science*, vol. 285, pp. 1537-1539, 1999.
- [27] P. S. J. Russell, "Photonic-crystal fibers," *IEEE J. Lightwave Technol.*, Journal of, vol. 24, pp. 4729-4749, 2006.
- [28] W. Jin, H. F. Xuan, and H. L. Ho, "Sensing with hollow-core photonic bandgap fibers," *Meas. Sci. Technol.*, vol. 21, p. 094014, 2010.
- [29] W. Belardi and J. C. Knight, "Hollow antiresonant fibers with low bending loss," *Opt. Express*, vol. 22, pp. 10091-10096, 2014.
- [30] P. Uebel, M. C. Günendi, M. H. Frosz, G. Ahmed, N. N. Edavalath, J.-M. Ménard, et al., "Broadband robustly single-mode hollow-core PCF by resonant filtering of higher-order modes," *Opt. Lett.*, vol. 41, pp. 1961-1964, 2016.
- [31] Y. Chen, Z. Liu, S. R. Sandoghchi, G. T. Jasion, T. D. Bradley, E. Numkam Fokoua, et al., "Multi-kilometer long, longitudinally uniform hollow core photonic bandgap fibers for broadband low latency data transmission," *IEEE J. Lightwave Technol.*, vol. 34, pp. 104-113, 2016.
- [32] P. Roberts, F. Couny, H. Sabert, B. Mangan, D. Williams, L. Farr, et al., "Ultimate low loss of hollow-core photonic crystal fibres," *Opt. Express*, vol. 13, pp. 236-244, 2005.
- [33] B. Mangan, L. Farr, A. Langford, P. J. Roberts, D. P. Williams, F. Couny, et al., "Low loss (1.7 dB/km) hollow core photonic bandgap fiber," in *Optical Fiber Communication Conference*, Los Angeles, California, 2004, p. PD24.
- [34] F. Benabid and P. J. Roberts, "Linear and nonlinear optical properties of hollow core photonic crystal fiber," *J. Mod. Opt.*, vol. 58, pp. 87-124, 2011.
- [35] P. S. J. Russell, P. Holzer, W. Chang, A. Abdolvand, and J. C. Travers, "Hollow-core photonic crystal fibres for gas-based nonlinear optics," *Nat. Photon.*, vol. 8, pp. 278-286, 2014.
- [36] A. D. Pryamikov, A. S. Biriukov, A. F. Kosolapov, V. G. Plotnichenko, S. L. Semjonov, and E. M. Dianov, "Demonstration of a waveguide regime for a silica hollow - core microstructured optical fiber with a negative curvature of the core boundary in the spectral region > 3.5 μm ," *Opt. Express*, vol. 19, pp. 1441-1448, 2011.
- [37] A. Hartung, J. Kobelke, A. Schwuchow, J. Bierlich, J. Popp, M. A. Schmidt, et al., "Low-loss single-mode guidance in large-core antiresonant hollow-core fibers," *Opt. Lett.*, vol. 40, pp. 3432-3435, 2015.
- [38] N. V. Wheeler, T. D. Bradley, J. R. Hayes, M. A. Gouveia, Y. Chen, S. R. Sandoghchi, et al., "Low loss Kagome fiber in the 1 μm wavelength region," in *Advanced Photonics 2016 (IPR, NOMA, Sensors, Networks, SPPCom, SOF)*, Vancouver, 2016, p. SoM3F.2.
- [39] W. A. Challener, N. Choudhury, J. Karp, A. M. Kasten, S. Palit, G. Pickrell, et al., "Gas sensing with hollow core fiber for leak detection and localization," in *Conference on Lasers and Electro-Optics*, San Jose, California, 2016, p. AW1J.1.
- [40] Y. L. Hoo, W. Jin, H. L. Ho, J. Ju, and D. N. Wang, "Gas diffusion measurement using hollow-core photonic bandgap fiber," *Sens. Actuators B-Chem.*, vol. 105, pp. 183-186, 2005.
- [41] T. Ritari, J. Tuominen, H. Ludvigsen, J. Petersen, T. Sørensen, T. Hansen, et al., "Gas sensing using air-guiding photonic bandgap fibers," *Opt. Express*, vol. 12, pp. 4080-4087, 2004.
- [42] A. van Brakel, C. Jáuregui Misas, T. T. Ng, P. Petropoulos, J. P. Dakin, C. Grivas, et al., "Cavity ring-down in a photonic bandgap fiber gas cell," in *Conference on Lasers and Electro-Optics/Quantum Electronics and Laser Science Conference and Photonic Applications Systems Technologies*, San Jose, California, 2008, p. CThEE4.
- [43] D. Munzke, B. M. x00F, hm, and O. Reich, "Gaseous oxygen detection using hollow-core fiber-based linear cavity ring-down spectroscopy," *IEEE J. Lightwave Technol.*, vol. 33, pp. 2524-2529, 2015.
- [44] K. S. Lee, Y. K. Lee, and S. H. Jang, "A novel grating modulation technique for photonic bandgap fiber gas sensors," *IEEE Photon. Technol. Lett.*, vol. 23, pp. 624-626, 2011.
- [45] A. M. Cubillas, M. Silva-Lopez, J. M. Lazaro, O. M. Conde, M. N. Petrovich, and J. M. Lopez-Higuera, "Methane detection at 1670-nm band using a hollow-core photonic bandgap fiber and a multiline algorithm," *Opt. Express*, vol. 15, pp. 17570-17576, 2007.
- [46] R. M. Wynne, B. Barabadi, K. J. Creedon, and A. Ortega, "Sub-minute response time of a hollow-core photonic bandgap fiber gas sensor," *IEEE J. Lightwave Technol.*, vol. 27, pp. 1590-1596, 2009.
- [47] H. Lehmann, H. Bartelt, R. Willsch, R. Amezcua-Correa, and J. C. Knight, "In-line gas sensor based on a photonic bandgap fiber with laser-drilled lateral microchannels," *IEEE Sens. J.*, vol. 11, pp. 2926-2931, 2011.
- [48] L. Xuefeng, L. Jinxing, L. Shuo, Y. Zimin, Z. Yupeng, and T. Ueda, "NIR Spectrum Analysis of Natural Gas Based on Hollow-Core Photonic Bandgap Fiber," *IEEE Sens. J.*, vol. 12, pp. 2362-2367, 2012.
- [49] F. Magalhaes, J. P. Carvalho, L. A. Ferreira, F. M. Araujo, and J. L. Santos, "Methane detection system based on Wavelength Modulation Spectroscopy and hollow-core fibres," in *IEEE Sensors*, 2008, pp. 1277-1280.
- [50] A. Simonsen, J. Hald, J. Lyngsø, and J. C. Petersen, "Hollow core photonic crystal fibers for quantitative measurements of fractional amounts of gases," in *OSA Imaging and Applied Optics Technical Digest 2012*, p. STu2F.2.
- [51] J. A. Nwaboh, J. Hald, J. K. Lyngsø, J. C. Petersen, and O. Werhahn, "Measurements of CO₂ in a multipass cell and in a hollow-core photonic bandgap fiber at 2 μm ," *Appl. Phys. B-Lasers Opt.*, pp. 1-8, 2012.
- [52] S. Do Lim, K. Ma, J. H. Jeong, G. Kim, K. Lee, J.-M. Jeong, et al., "In situ gas sensing using a remotely detectable probe with replaceable insert," *Opt. Express*, vol. 20, pp. 1727-1732, 2012.
- [53] A. M. Cubillas, J. M. Lazaro, M. Silva-Lopez, O. M. Conde, M. N. Petrovich, and J. m. Lopez-Higuera, "Methane sensing at 1300 nm band with hollow-core photonic bandgap fibre as gas cell," *Electron. Lett.*, vol. 44, pp. 403-404, 2008.
- [54] A. Cubillas, J. Lazaro, O. Conde, M. Petrovich, and J. Lopez-Higuera, "Multi-line fit model for the detection of methane at v₂ + 2v₃ band using hollow-core photonic bandgap fibres," *Sensors*, vol. 9, p. 490, 2009.
- [55] J. P. Parry, B. C. Griffiths, N. Gayraud, E. D. McNaghten, A. M. Parkes, W. N. MacPherson, et al., "Towards practical gas sensing with micro-structured fibres," *Meas. Sci. Technol.*, vol. 20, p. 075301, 2009.
- [56] Y. L. Hoo, L. Shujing, H. Hoi Lut, and J. Wei, "Fast response microstructured optical fiber methane sensor with multiple side-openings," *IEEE Photon. Technol. Lett.*, vol. 22, pp. 296-298, 2010.
- [57] T. P. Hansen, J. Broeng, C. Jakobsen, G. Vienne, H. R. Simonsen, M. D. Nielsen, et al., "Air-guiding photonic bandgap fibers: spectral properties,

- macro-bending loss, and practical handling," *IEEE J. Lightwave Technol.*, vol. 22, p. 11, 2004.
- [58] M. N. Petrovich, F. Poletti, and D. J. Richardson, "Analysis of modal interference in photonic bandgap fibres," in *12th International Conference on Transparent Optical Networks*, 2010, pp. 1-4.
- [59] M. N. Petrovich, F. Poletti, A. van Brakel, and D. J. Richardson, "Robustly single mode hollow core photonic bandgap fiber," *Opt. Express*, vol. 16, pp. 4337-4346, 2008.
- [60] J. M. Fini, J. W. Nicholson, B. Mangan, L. Meng, R. S. Windeler, E. M. Monberg, et al., "Polarization maintaining single-mode low-loss hollow-core fibres," *Nat. Commun.*, vol. 5, 2014.
- [61] Y. Wang, W. Jin, J. Ju, H. Xuan, H. L. Ho, L. Xiao, et al., "Long period gratings in air-core photonic bandgap fibers," *Opt. Express*, vol. 16, pp. 2784-2790, 2008.
- [62] F. Yang, W. Jin, Y. Cao, H. L. Ho, and Y. Wang, "Towards high sensitivity gas detection with hollow-core photonic bandgap fibers," *Opt. Express*, vol. 22, pp. 24894-24907, 2014.
- [63] G. Stewart, A. Mencaglia, W. Philip, and J. Wei, "Interferometric signals in fiber optic methane sensors with wavelength modulation of the DFB laser source," *IEEE J. Lightwave Technol.*, vol. 16, pp. 43-53, 1998.
- [64] H. C. Sun and E. A. Whittaker, "Novel étalon fringe rejection technique for laser absorption spectroscopy," *Appl. Opt.*, vol. 31, pp. 4998-5002, 1992.
- [65] W. Jin, Y. Z. Xu, M. S. Demokan, and G. Stewart, "Investigation of interferometric noise in fiber-optic gas sensors with use of wavelength modulation spectroscopy," *Appl. Opt.*, vol. 36, pp. 7239-7246, 1997.
- [66] J. W. Nicholson, L. Meng, J. M. Fini, R. S. Windeler, A. DeSantolo, E. Monberg, et al., "Measuring higher-order modes in a low-loss, hollow-core, photonic-bandgap fiber," *Opt. Express*, vol. 20, pp. 20494-20505, 2012.
- [67] L. Xiao, W. Jin, and M. S. Demokan, "Fusion splicing small-core photonic crystal fibers and single-mode fibers by repeated arc discharges," *Opt. Lett.*, vol. 32, pp. 115-117, 2007.
- [68] L. Xiao, M. S. Demokan, W. Jin, Y. Wang, and C.-L. Zhao, "Fusion splicing photonic crystal fibers and conventional single-mode fibers: microhole collapse effect," *IEEE J. Lightwave Technol.*, vol. 25, pp. 3563-3574, 2007.
- [69] H. Lehmann, S. Brueckner, J. Kobelke, G. Schwotzer, K. Schuster, and R. Willsch, "Toward photonic crystal fiber based distributed chemosensors." In *Proc. SPIE 5855, 17th International Conference on Optical Fibre Sensors*, 2005, pp. 419-422.
- [70] C. M. B. Cordeiro, E. M. dos Santos, C. H. Brito Cruz, C. J. S. de Matos, and D. S. Ferreira, "Lateral access to the holes of photonic crystal fibers – selective filling and sensing applications," *Opt. Express*, vol. 14, pp. 8403-8412, 2006.
- [71] L. Xuefeng, P. Joanna, L. Jinxing, X. Guan, and U. Toshitsugu, "Fabrication of photonic bandgap fiber gas cell using focused ion beam cutting," *Jpn. J. Appl. Phys.*, vol. 48, p. 06FK05, 2009.
- [72] L. Xuefeng, L. Jinxing, O. Hiroshi, and U. Toshitsugu, "Doubled optical path length for photonic bandgap fiber gas cell using micromirror," *Jpn. J. Appl. Phys.*, vol. 50, p. 06GM01, 2011.
- [73] C. J. Hensley, D. H. Broaddus, C. B. Schaffer, and A. L. Gaeta, "Photonic band-gap fiber gas cell fabricated using femtosecond micromachining," *Opt. Express*, vol. 15, pp. 6690-6695, 2007.
- [74] A. van Brakel, C. Grivas, M. N. Petrovich, and D. J. Richardson, "Micro-channels machined in microstructured optical fibers by femtosecond laser," *Opt. Express*, vol. 15, pp. 8731-8736, 2007.
- [75] A. Heilig, N. Bârsan, U. Weimar, M. Schweizer-Berberich, J. W. Gardner, and W. Göpel, "Gas identification by modulating temperatures of SnO₂-based thick film sensors," *Sens. Actuators B-Chem.*, vol. 43, pp. 45-51, 1997.
- [76] S. E. Bialkowski, *Photothermal Spectroscopy Methods for Chemical Analysis*. New York: Wiley, 1996.
- [77] C. C. Davis and S. J. Petuchowski, "Phase fluctuation optical heterodyne spectroscopy of gases," *Appl. Opt.*, vol. 20, pp. 2539-2554, 1981.
- [78] M. A. Owens, C. C. Davis, and R. R. Dickerson, "A photothermal interferometer for gas-phase ammonia detection," *Anal. Chem.*, vol. 71, pp. 1391-1399, 1999.
- [79] N. D. Weston, P. Sakthivel, and P. Mukherjee, "Ultrasensitive spectral trace detection of individual molecular components in an atmospheric binary mixture," *Appl. Opt.*, vol. 32, pp. 828-835, 1993.
- [80] D. L. Mazzoni and C. C. Davis, "Trace detection of hydrazines by optical homodyne interferometry," *Appl. Opt.*, vol. 30, pp. 756-764, 1991.
- [81] A. Sedlacek and J. Lee, "Photothermal interferometric aerosol absorption spectrometry," *Aerosol Sci. Technol.*, vol. 41, pp. 1089-1101, 2007.
- [82] J. A., Campillo, "Fabry-Perot photothermal trace detection," *Appl. Phys. Lett.*, vol. 41, pp. 327-329, 1982.
- [83] F. Yang, W. Jin, Y. Cao, and H. L. Ho, "Photothermal effect in gas-filled hollow-core photonic bandgap fiber," in *Proc. SPIE 9634, 24th International Conference on Optical Fibre Sensors*, 2015, pp. 96340W-96340W-4.
- [84] Y. Cao, W. Jin, F. Yang, and H. L. Ho, "Phase sensitivity of fundamental mode of hollow-core photonic bandgap fiber to internal gas pressure," *Opt. Express*, vol. 22, pp. 13190-13201, 2014.
- [85] D. A. Jackson, R. Priest, A. Dandridge, and A. B. Tveten, "Elimination of drift in a single-mode optical fiber interferometer using a piezoelectrically stretched coiled fiber," *Appl. Opt.*, vol. 19, pp. 2926-2929, 1980.
- [86] K. P. Koo, A. B. Tveten, and A. Dandridge, "Passive stabilization scheme for fiber interferometers using (3×3) fiber directional couplers," *Appl. Phys. Lett.*, vol. 41, pp. 616-618, 1982.
- [87] K. Kråkenes and K. Bløtækjaer, "Sagnac interferometer for underwater sound detection: noise properties," *Opt. Lett.*, vol. 14, pp. 1152-1154, 1989.
- [88] K. K. Clay and D. Anthony, "Overview of high performance fibre-optic sensing," *J. Phys. D-Appl. Phys.*, vol. 37, p. R197, 2004.
- [89] A. Dandridge, "Fiber optic sensors based on the Mach-Zehnder and Michelson interferometers," in *Fiber Optic Sensors*, ed: John Wiley & Sons, Inc., 2011, pp. 231-275.
- [90] K. S. Kim, W. A. Reed, K. W. Quoi, and R. H. Stolen, "Measurement of the nonlinear index of silica-core and dispersion-shifted fibers," *Opt. Lett.*, vol. 19, pp. 257-259, 1994.
- [91] V. Dangui, M. J. F. Dignonnet, and G. S. Kino, "Laser-driven photonic-bandgap fiber optic gyroscope with negligible Kerr-induced drift," *Opt. Lett.*, vol. 34, pp. 875-877, 2009.
- [92] F. Yang and W. Jin, "In-fiber modal interferometer for high sensitivity gas detection," in *Proc. SPIE 9634, 24th International Conference on Optical Fibre Sensors*, 2015, pp. 963410-963410-4.
- [93] F. Yang, Y. Tan, W. Jin, Y. Lin, Y. Qi, and H. L. Ho, "Hollow-core fiber Fabry-Perot photothermal gas sensor," *Opt. Lett.*, vol. 41, pp. 3025-3028, 2016.
- [94] R. L. McCreery, "Magnitude of Raman scattering," in *Raman Spectroscopy for Chemical Analysis*, ed: John Wiley & Sons, Inc., 2005, pp. 15-33.
- [95] J. P. Carvalho, H. Lehmann, H. Bartelt, F. Magalhaes, R. Amezcua-Correa, J. L. Santos, et al., "Remote system for detection of low-levels of methane based on photonic crystal fibres and wavelength modulation spectroscopy," *J. Sens.*, vol. 2009, p. 10, 2009.
- [96] M. N. Petrovich, A. M. Heidt, N. V. Wheeler, N. K. Baddela, and D. J. Richardson, "High sensitivity methane and ethane detection using low-loss mid-IR hollow-core photonic bandgap fibers," in *Proc. SPIE 9157, 23rd International Conference on Optical Fibre Sensors*, 2014, pp. 91573P-91573P-4.
- [97] M. P. Buric, K. P. Chen, J. Falk, and S. D. Woodruff, "Improved sensitivity gas detection by spontaneous Raman scattering," *Appl. Opt.*, vol. 48, pp. 4424-4429, 2009.
- [98] J. L. Doménech and M. Cueto, "Sensitivity enhancement in high resolution stimulated Raman spectroscopy of gases with hollow-core photonic crystal fibers," *Opt. Lett.*, vol. 38, pp. 4074-4077, 2013.
- [99] P. G. Westergaard, M. Lassen, and J. C. Petersen, "Differential high-resolution stimulated CW Raman spectroscopy of hydrogen in a hollow-core fiber," *Opt. Express*, vol. 23, pp. 16320-16328, 2015.
- [100] L. S. Rothman, I. E. Gordon, Y. Babikov, A. Barbe, D. Chris Benner, P. F. Bernath, et al., "The HITRAN 2012 molecular spectroscopic database," *J. Quant. Spectrosc. Radiat. Transf.*, vol. 130, pp. 4-50, 2013.